Stability and Dynamics of G-Actin: Back-Door Water Diffusion and Behavior of a Subdomain 3/4 Loop

Willy Wriggers and Klaus Schulten
Department of Physics, Beckman Institute, University of Illinois at Urbana-Champaign, Urbana, Illinois 61801 USA

ABSTRACT Molecular dynamics simulations have been performed on solvated G-actin bound to ADP and ATP, starting with the crystal structure of the actin-DNase 1 complex, including a Ca^{2+} or Mg^{2+} ion at the high-affinity divalent cation-binding site. Water molecules have been found to enter the nucleotide-binding site (phosphate vicinity) along two pathways, from the side where the nucleotide base is exposed to water, as well as from the opposite side. The water channels suggest a "back-door" mechanism for ATP hydrolysis in which the phosphate is released to a side opposite that of nucleotide binding and unbinding. The simulations also reveal a propensity of G-actin to alter its crystallographic structure toward the filamentous structure. Domain movement closes the nucleotide cleft, the movement being more pronounced for bound Mg^{2+}. The conformational change is interpreted as a response of the system to missing water molecules in the crystal structure. The structures arising in the simulations, classified according to nucleotide cleft separation and radius of gyration of the protein, fall into two distinct clusters: a cluster of states that are similar to the G-actin crystal structure, and a cluster of states with small cleft separation and with the subdomain 3/4 loop 264–273 detached from the protein. The latter states resemble the putative filamentous structure of actin, in which the loop connects the two strands of the actin filament.

INTRODUCTION

Actin comprises 375 amino acid residues, organized in four subdomains (Kabsch et al., 1990), which give the protein a cloverleaf appearance. G-actin (globular actin) monomers can aggregate, forming a two-start helix of (filamentous) F-actin (Holmes et al., 1990). Actin filaments are dynamic polymers, whose assembly and disassembly in the cytoplasm drive shape changes (Small, 1989), cell locomotion (Theriot et al., 1992), and chemotactic migration (Devreotes and Zigmond, 1988). The elongation of the filament is accompanied by the hydrolysis of ATP, the fundamental carrier of metabolic energy in the cell (Carlier, 1991). Actin ATPase activity is not required for aggregation, but is believed to serve as a destabilizing reaction to promote the depolymerization of the resulting ADP-bound filament (Pollard et al., 1992). Associated with the nucleotide is a tightly bound divalent cation that can be Ca^{2+} or Mg^{2+} (Frieden et al., 1980). In this work we investigate, by molecular dynamics (MD) simulation (Levitt, 1983; Brooks et al., 1983), the behavior of an actin structure (Kabsch et al., 1990) in solution, and suggest structure and function relationships relevant to the polymerization and ATPase activity of the protein.

Theoretical studies of actin by us and other groups seek to provide an understanding of actin's dynamics and functional activity. A normal-mode analysis of G-actin provided insight into the intrinsic flexibility of the protein (Tirion and ben-Avraham, 1993). An MD simulation of G-actin without nucleotide and divalent cation was undertaken by Suda and Saito (1994). In the present work, MD simulations are carried out that include ADP and ATP as well as a divalent cation.

Water molecules that are buried inside a protein often constitute integral parts of its structure (Zhang and Hermans, 1996). Specific binding sites of water molecules in actin have not been suggested, because of the limited (>2.5 Å) resolution of the available crystal structures (Kabsch et al., 1990; Schutt et al., 1993; McLaughlin et al., 1993; Chik et al., 1996). However, a 1.7-Å resolution structure of another ATPase, the 44-kDa fragment of the chaperone Hsc70, was recently determined (Wilbanks and McKay, 1995). Although there is little sequence identity, the structures of actin and the Hsc70 fragment were found to be similar (Flaherty et al., 1991). The authors superimposed 241 pairs of equivalent residues with a rms difference of 2.3 Å, found similar ADP-binding pockets in both structures, and could identify a universal sequence "fingerprint" for the nucleotide-binding pocket. More importantly, the new high-resolution structure of the 44-kDa ATPase fragment reveals several buried water molecules and two monovalent ions in the vicinity of the nucleotide (Flaherty et al., 1994; Wilbanks and McKay, 1995), raising the question of whether actin's structure contains buried water molecules and monovalent ions as well. MD simulations, which allow one to study the short-time dynamics of biomolecules at atomic resolution, are especially suitable for the study of diffusing water molecules in narrow channels (Breed et al., 1996). In this work we investigate the hydration of actin's enzymatic site and study water diffusion pathways that may be relevant for substrate exchange in ATP hydrolysis.

Mechanical properties of filamentous actin can be altered by actin-binding agents. Phalloidin, a heptapeptide toxin

Received for publication 12 December 1996 and in final form 10 May 1997.

Address reprint requests to Dr. Klaus Schulten, Department of Physics, Beckman Institute 3147, University of Illinois at Urbana-Champaign, 405 N. Mathews Ave., Urbana, IL 61801. Tel.: 217-244-1604; Fax: 217-244-6078; E-mail: kschulte@ks.uiuc.edu.

0006-3495/97/08/624/16 $2.00

from the mushroom *Amanita phalloides*, is often used to stabilize F-actin in vitro. The toxin prevents monomer dissociation at both ends of the polymer (Estes et al., 1981; Coluccio and Tilney, 1984; Sampath and Pollard, 1991) and stiffens the filament (Isambert et al., 1995). Fig. 1 presents the Lorenz F-actin model, which predicts the phalloidin-binding site in the filament (Lorenz et al., 1993). In this model, phalloidin contacts three actin monomers simultaneously, which provides a rationale for its stabilizing function. Phalloidin binding to actin has also been shown to delay the release of inorganic phosphate after ATP hydrolysis, which accompanies the polymerization (Dancker and Hess, 1990). Conversely, no effect of inorganic phosphate on the phalloidin binding kinetics has been observed (De La Cruz and Pollard, 1994). The influence of phalloidin on the phosphate kinetics without the phosphate affecting phalloidin appears to be a paradox. We seek to understand the structural mechanism of phosphate release, which would clarify the manner in which phosphate and phalloidin interact.

Two aspects of actin's dynamics are relevant for the conformational transition during polymerization (G-F transition). First, a closure of the nucleotide-binding cleft, which separates subdomain 2 from subdomain 4, was suggested to be associated with the polymerization of actin into filaments (Lorenz et al., 1993; Tirion et al., 1995). Second, the G-F transition presumably is also accompanied by the detachment of loop 264–273 at the interface of subdomains 3 and 4. Holmes et al. (1990) used computer modeling to rebuild loop 264–273 into a β-hairpin to form a projecting element that would fit into a hydrophobic pocket between the two monomers on the opposite strand of the actin filament (Fig. 1). The "hydrophobic plug" is only a hypothesis, but it has received considerable support from mutational experiments (Chen et al., 1993; Kuang and Rubenstein, 1997a; Kuang and Rubenstein, 1997b). In the G-actin crystal structure, the loop makes contact with the main body of the actin molecule via a hydrophobic interaction of Phe^{266} with Met^{227}, Phe^{223} and the methylenes of Arg^{256} and Glu^{259}. In the Kabsch structure, this hydrophobic interaction is disturbed by the carboxylate side chain of Glu^{259} (Kabsch et al., 1990). In the actin:profilin and actin:gelsolin-subfragment 1 structures (Schutt et al., 1993; McLaughlin et al., 1993), Glu^{259} formes a salt bridge with Arg^{312}, and Phe^{266} appears to be part of a hydrophobic cluster (see figure 2 *d* of Schutt et al., 1993). Schutt et al. (1994) argued that, according to their structure, a considerable energy barrier would have to be overcome to detach the loop from the protein. To date, the conformation of the hydrophobic plug loop is still the subject of controversy, and MD

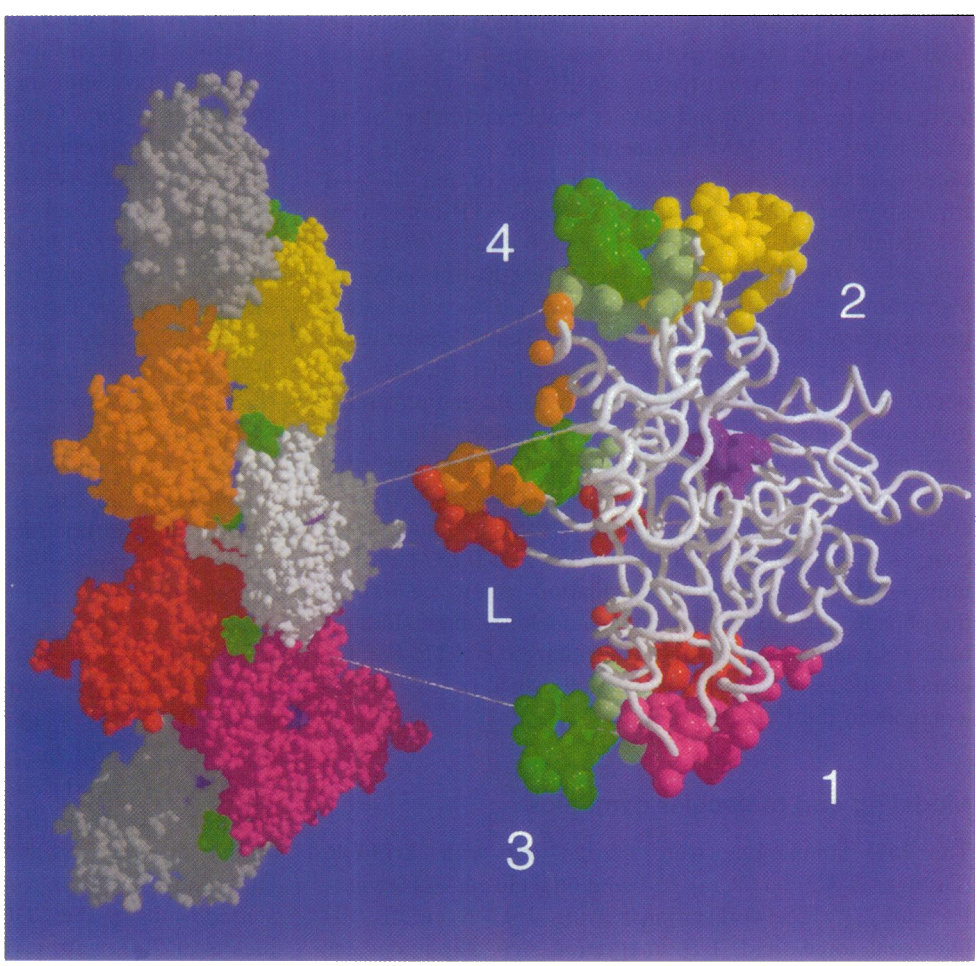

FIGURE 1 Lorenz F-actin model with phalloidin (Lorenz et al., 1993) (*left*) and contact regions in the monomer (*right*), visualized by Radiance (Ward, 1994). Phalloidin peptides are shown in green, ADP nucleotides in purple. The enlarged monomer highlights interactin contacts and actin-phalloidin contacts (*solid sphere representation*). The color of the spheres codes for the neighboring monomer or phalloidin in the filament (*left*). Of special interest is the hydrophobic plug loop (L), which connects the two strands of the filament by interacting with two opposing monomers (*red, orange*). Each phalloidin molecule interacts with three actin monomers. The indices 1–4 identify actin's structural subdomains.

simulations can be employed to investigate the suggested scenarios.

In the following we describe the modeling of the hydrated protein in the presence of nucleotide and cation. Subsequently, in Results and Discussion, we present our findings, including possible channels permitting entry and exit of water, ions, and substrates to the enzymatic site; the role of nucleotide hydration; and a scenario for the release of the putative "hydrophobic plug" loop. The implications of our results for actin's function in cell motility are described in Summary and Conclusions.

COMPUTATIONAL METHODS

In this section we outline our method of nucleotide parameterization and the MD protocols used to model the dynamics of monomeric actin in solution. Subsequently, we describe methods used to identify domain movements and radial displacements of residues in the analysis of the resulting simulated structures.

Nucleotide parameterization

For the MD simulations we used the program X-PLOR (Brünger, 1992), version 3.1, with the CHARMM (Brooks et al., 1983) all-hydrogen force field, version 22. Because this force field does not include standard parameters for ADP and ATP, the nucleotides were modeled as follows: available standard from Quanta (MSI, 1994), version 4.0, were used for the bond and van der Waals parameters of the phosphates; CHARMM parameters of the nucleotide adenine were used for the sugar and base of the di- and triphosphates; partial charges for ADP and ATP atoms were calculated by means of Gaussian (Frisch et al., 1992), version 92, at the Hartree-Fock level (Merz-Kollmann/Singh algorithm), using a 6-31 G* basis set for the nucleotide geometries of Kabsch et al. (1990) (ATP) and Lorenz et al. (1993) (ADP). (The topology and parameter files for the nucleotides are available via anonymous ftp at ftp://ftp.ks.uiuc.edu/ in directory/pub/projects/nucleotide.) The calculated charges for the base and sugar of the nucleotide were found to be in good agreement with the standard CHARMM adenine charges [the rms difference of the individual partial charges is 0.1472 charge units (ADP) and 0.1374 charge units (ATP)]. The *ab initio* calculations improved mostly the phosphate charges compared to adenine, maintaining a total -3 charge on ADP and a -4 charge on ATP. Parameters for the associated divalent cation (Mg^{2+} or Ca^{2+}) were available in the CHARMM force field.

Modeling and molecular dynamics

The MD simulations were carried out with X-PLOR (Brünger, 1992) on a Cray C90 and on a cluster of Hewlett-Packard 735/125 workstations, using a 12-Å cutoff, all-hydrogen force field, 1-fs integration step, explicit water molecules, and a dielectric constant of $\epsilon = 1$. For the simulation, the protonation degree of the histidine residues of G-actin was estimated based on their stability: His^{371}, His^{101}, His^{88}, and His^{275} are stabilized by hydroxyl or carboxyl groups and were simulated in the doubly protonated state; His^{40}, His^{87}, His^{173}, His^{161}, and the methylated His^{73} were simulated as singly protonated. Residues 373–375, which are missing in the Kabsch crystal structure (Kabsch et al., 1990), were added to the model by using coordinates from Lorenz et al. (1993); a short simulated annealing protocol of 1 ps was performed to relax their conformation, while keeping the remaining residues 1–372 fixed. The completed protein was then solvated in a 5.6-Å shell of 1189 water molecules. The choice of this simple solvent model follows the method of Steinbach and Brooks (1993); these authors demonstrated that the protein myoglobin (2536 atoms) is hydrated satisfactorily by ~350 water molecules and that only a moderate number of water molecules are required in simulations of globular proteins, mainly to hydrate charged surface groups. The TIP3P water model (Jorgensen et al., 1983) was used, however, modified by omitting internal geometry constraints to provide water flexibility. This modification was motivated by MD studies that demonstrate an improvement of physical properties of flexible water over the rigid TIP3 model (Teeter, 1991; Daggett and Levitt, 1993). Flexible TIP3P water exhibits values for the water density, heat of vaporization, and diffusion coefficient as close to the experimental values as those obtained with the original TIP3P model (Steinbach and Brooks, 1993; Guàrdia and Padró, 1996).

The total system size is 9441 atoms (ADP-actin) and 9445 atoms (ATP-actin). The systems were first minimized, then assigned initial velocities according to a Maxwell distribution, heated up to 300 K in steps of 30 K in a 5-ps time period, and equilibrated at 300 K for 5 ps. Finally, free molecular dynamics was performed. Translational and rotational rigid body degrees of freedom were eliminated from the trajectories by least-squares fitting (Kabsch, 1976) of the frames to the respective initial structures. Structures after 300-ps and 500-ps simulation time were extracted from the trajectories after averaging over 5 ps, to remove fast thermal fluctuations, and after a subsequent energy minimization to adjust unnatural bond lengths and bond angles.

For the present investigation, we simulated G-actin with bound ADP, ATP, and either Ca^{2+} or Mg^{2+} ions (labeled Ca-ADP, Mg-ADP, Ca-ATP, and Mg-ATP). Four respective trajectories of 500-ps simulation time, for Ca-ADP, Mg-ADP, Ca-ATP, and Mg-ATP, will be referred to as CDC, CDM, CTC, and CTM, respectively. To investigate the dependence of the protein conformation on the initial condition we produced, in addition to CDM, a second, 300-ps trajectory of Mg-ADP-actin, termed CDN, starting with a different assignment of initial velocities. Finally, CDm and CTm are trajectories of 200-ps length, which were started by using the CDC and CTC coordinates and velocities after 300 ps, to investigate the effect of replacing the

Ca^{2+} ion by Mg^{2+}. An overview of the seven trajectories is given in Table 1.

All simulations were started from the Kabsch crystal structures with bound ADP and ATP (Kabsch et al., 1990). The two structures are very similar (their mutual rms deviation of 0.4 Å is well below the 2.5-Å crystallographic resolution). If necessary, we will differentiate between ATP-bound G-actin from the Brookhaven Protein Data Bank entry 1ATN, which will be denoted KAT, and the ADP-bound structure (provided by W. Kabsch), which will be referred to as KAD.

Besides the Kabsch crystal structures, three other actin structures were available for comparison with the simulation results: 1) the crystal structure of the actin-profilin complex (Schutt et al., 1993), denoted in this paper as SCH; 2) the F-actin model of Lorenz et al. (1993), denoted as LOR; 3) the F-actin model of Tirion et al. (1995), denoted as TIR.

Identifying rigid domains

Rigid domains in actin were determined with the Hingefind algorithm (Wriggers and Schulten, 1997). The algorithm compares two known structures and partitions the protein, with a prespecified resolution, in connected regions of preserved packing. A rigid region is found in an iterative adaptive selection procedure, in which poor matching residues are excluded from the domain and good matches are included. The algorithm then determines effective hinge axes and rotation angles that characterize the relative movements of the domains. We extracted rigid domains from a comparison of a simulated structure relative to the initial crystal structure and from a comparison of the Lorenz F-actin model relative to the crystal structure. An optimum resolution was chosen to filter the significant movements from noise and thermal disorder (cf. Results and Discussion).

Radial differences of structures

It is often desirable to investigate conformational differences in a comparison of two structures locally, e.g., as a function of the residue number. Here we are only interested in the radial component of conformational differences between structures. Let $\vec{x}_i$ and $\vec{x}_i'$ ($i = 1, 2, \ldots, N$) be two given vector sets of atom positions and m_i be the mass of each atom i. For simplicity we assume that $\vec{x}_i$ and $\vec{x}_i'$ ($i = 1, 2, \ldots, N$) have their center of mass translated to the origin. The radius of gyration,

$$r_{gyr} = \sqrt{\frac{1}{M}\sum_{i=1}^{N} m_i r_i^2} \quad (r_i = |\vec{x}_i|) \tag{1}$$

is a standard measure for the compactness of the protein structure. For each atom i the radial difference in position is given by

$$\Delta r_i = r_i' - r_i \tag{2}$$

To measure the contribution of each residue to the changes in the radius of gyration, we expand Eq. 1 to first order about the atom radii r_i:

$$r_{gyr}(\{r_i'\}) = r_{gyr}(\{r_i\}) + \sum_{i=1}^{N} \Delta r_{gyr}(i) + \mathcal{O}(\Delta r_i^2) \tag{3}$$

where $\Delta r_{gyr}(i)$ is

$$\Delta r_{gyr}(i) = \frac{\partial}{\partial r_i}\left(\sqrt{\frac{1}{M}\sum_{k=1}^{N} m_k r_k^2}\right)\Bigg|_{\{r_i\}} \Delta r_i = \frac{m_i r_i \Delta r_i}{M r_{gyr}(\{r_i\})} \tag{4}$$

Hence the contribution of each atom to changes in the radius of gyration is (in first order) given by its radial difference Δr_i, weighed by its mass m_i and radius r_i. To obtain a distribution of radial changes as a function of residue number, the first-order contributions of atoms were summed up for each residue.

RESULTS AND DISCUSSION

In this section we report the structural and dynamic properties of simulated G-actin. We compare the nucleotide-binding sites of crystal and simulated structures and of a structure of the 44-kDa ATPase fragment of the chaperone Hsc70, which closely resembles actin. We discuss the role of water molecules for the stability of the enzymatic site and the diffusion of water molecules in the vicinity of the nucleotide. In the remainder of the section, we give an account of the observed conformational changes and the structural similarity of certain simulated structures to F-actin.

TABLE 1 Overview of simulation trajectories

System	Nucleotide	Ion	Start structure	Sim. time (ps)
CDC	ADP	Ca^{2+}	KAD	500
CDM	ADP	Mg^{2+}	KAD	500
CTC	ATP	Ca^{2+}	KAT	500
CTM	ATP	Mg^{2+}	KAT	500
CDN	ADP	Mg^{2+}	KAD	300
CDm	ADP	Mg^{2+}	CDC (300 ps)	200
CTm	ATP	Mg^{2+}	CTC (300 ps)	200

Stability and dynamics of simulated structures

Measures commonly used to assess the stability and flexibility of systems in MD simulations are the rms deviation from the initial structure, the dependence of the conformation on the initial condition, and the rms fluctuations from the average structure. In Fig. 2 backbone rms deviations of CDC, CDM, CDN, CTC, and CTM are presented. Fig. 3 shows the dependence of α-carbon positions on the initial condition (CDN versus CDM) and the rms fluctuations of α-carbons (CDM only).

A comparison of the trajectories CDN and CDM, which were started from different initial velocities, reveals that the simulated structures are sensitive to the initial assignment of the velocities (Fig. 2). CDN stayed closer to the initial structure and stabilized at 3 Å rms deviation, whereas CDM drifted to rms differences of more than 4 Å. Structural differences between the trajectories can be larger than 10 Å for certain α-carbon positions (Fig. 3 *a*). Most of the α-carbon positions in the two trajectories, however, are preserved, exhibiting less than 2 Å deviation. Structural differences that are dependent on the initial condition can be attributed to movements of flexible secondary structure elements located on the surface of the protein (Fig. 3). The following flexible secondary structure elements can be identified: the DNase binding loop 38–52, the helix 223–230 in subdomain 4, loop 241–247 in subdomain 4, helix 309–320 in subdomain 3, and helices 350–355 and 359–365 near the C-terminus in subdomain 1. C_α atoms that are sensitive to the initial condition exhibit large rms fluctuations in their positions (Fig. 3 *b*) because of their exposure to the solvent, in good agreement with the results of other theoretical studies (Suda and Saito, 1994; Tirion and ben-Avraham, 1993).

Atomic fluctuations are related to crystal *B*-factors by $B = (8\pi^2/3)\,\langle(\Delta\mathbf{r})^2\rangle$, where $\Delta\mathbf{r}$ is the atomic displacement from the average position. Fig. 3 *b* compares the fluctuations computed from crystallographic *B*-factors (Kabsch et al., 1990) to fluctuations from simulation. It should be noted that MD simulations reproduce only intrinsic fluctuations of atoms, whereas crystallographic *B*-factors also include external, rigid body motions of the protein and static disorder in the crystal. Thus the crystal fluctuations are higher, except for residues 223–230 (solvent exposed helix) and 38–52 (DNase binding loop). The lower flexibility of these residues in the crystal may be due to crystal packing constraints and binding of DNase.

As shown in Fig. 2, backbone deviations from the initial structures lie between 2 and 4 Å for all trajectories. Most of the structural changes in actin occur within the first 10–20 ps of simulation time, indicating a fast relaxation from the crystal structure. In Suda and Saito (1994), the relaxation time was significantly longer (50 ps) and the rms difference somewhat smaller (1.7 Å) compared to our simulations, which include the nucleotide and the divalent cation. To find a structural basis for the fast relaxation from the crystal structure and the relatively large rms differences observed, we investigated the geometry of actin's nucleotide and ion-binding site.

In Fig. 4 the nucleotide-binding sites of the Kabsch ATP-actin structure, the final structure of CTC, and the Hsc70 ATPase fragment structure (Wilbanks and McKay, 1995), with bound ADP and inorganic phosphate, are com-

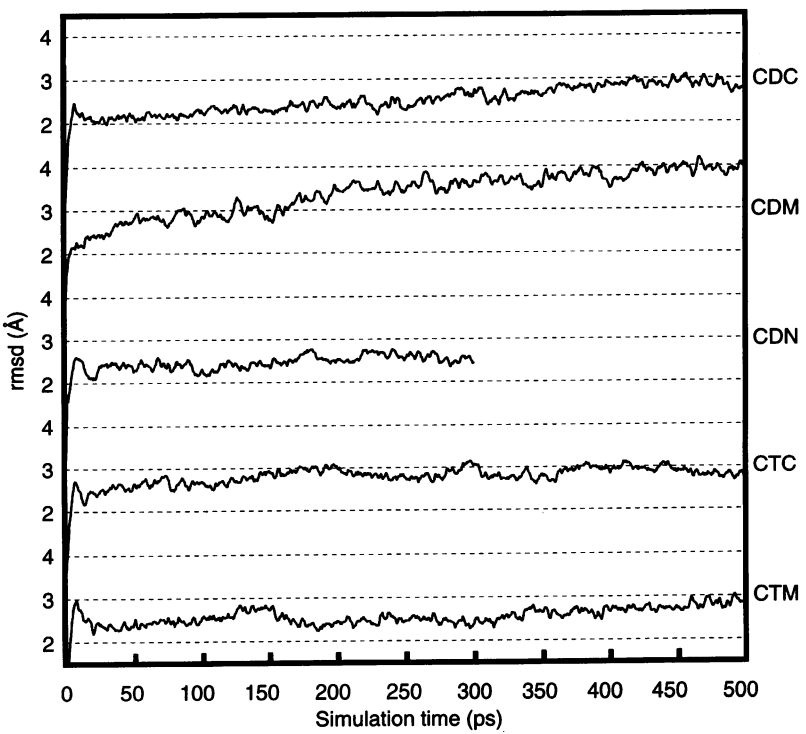

FIGURE 2 Backbone rms deviations from the respective initial structures as a function of simulation time. Deviations of the trajectories CDC, CDM, CDN, CTC, and CDM are compared.

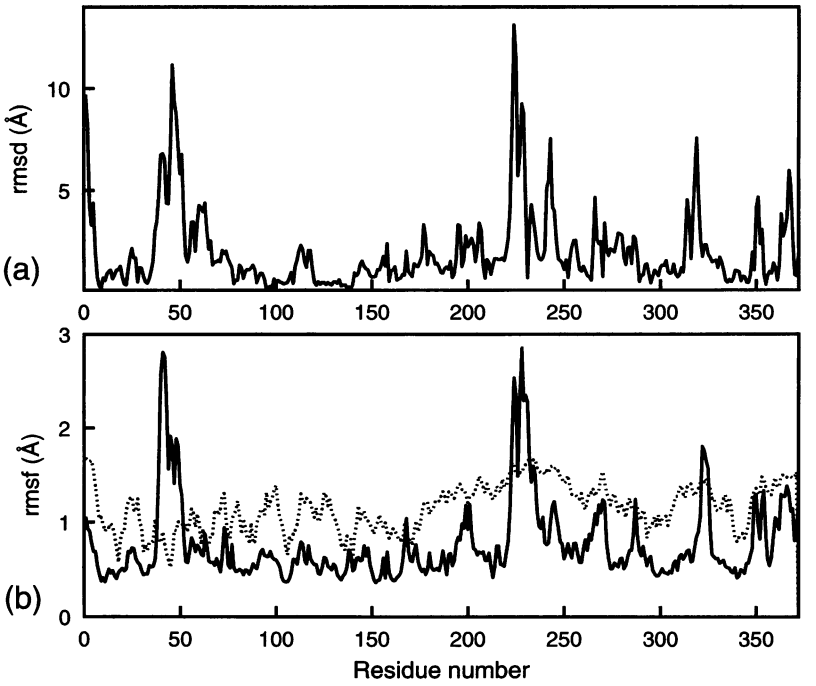

FIGURE 3 (*a*) C_α rms differences between trajectories CDN and CDM at 300 ps. (*b*) C_α rms fluctuations exhibited by CDM from 100 to 300 ps simulation time (——), and fluctuations calculated from crystal *B* factors (Kabsch et al., 1990) (·····).

pared. In the structure from CTC, Gln^{137} and Asp^{154} deviate from the crystal conformation, and the nucleotide-binding site appears compacted. Conversely, the nucleotide and divalent cation are stabilized by nine water molecules and two monovalent ions in Hsc70. Distances between nucleotide and residues in its binding pocket are similar to those found in the crystal structure of actin.

The compaction of the nucleotide-binding site in the simulated structures is further exemplified by the coordination of the divalent cation. Table 2 compares the coordination of the ion in the final structures of the trajectories CDC, CTC, CDM, and CTM to the coordination in the initial crystal structures (KAD and KAT). In the ATP-bound structures (from CTC and CTM) the ion is involved in interaction with Asp^{154} and Gln^{137}. Distances for Mg^{2+} are slightly smaller because of a smaller van der Waals ion radius of Mg^{2+} of (0.65 Å compared to the 0.99 Å of Ca^{2+}; Israelachvili, 1992). The compaction of the nucleotide-binding site is evident: Asp^{154} and Gln^{137} are at a smaller distance relative to KAT. The ion is coordinated to the α-, β-, and γ-phosphates of ATP, deviating from KAT, where it is only β-γ-coordinated. The situation is similar for the ADP-bound structures (from CDC and CDM). Interactions of the ion with Asp^{154} and Gln^{137} are stronger than in the crystal structure. The ion is coordinated to the α- and β-phosphates, whereas in KAD it is only β-coordinated.

The comparison with the 1.7-Å resolution crystal structure of Hsc70 suggests that in the actin crystal structure, certain solvent molecules that hydrate the enzymatic site may not have been detected at 2.5-Å resolution. We interprete the observed compaction of the enzymatic site in our simulation as an effect of incomplete hydration of the nucleotide vicinity in the Kabsch crystal structure, which served as a starting point for our simulations.

Water diffusion

Fig. 4 and Table 2 demonstrate that the absence of internal water molecules in the crystal structure causes a noticeable perturbation of simulated actin in the vicinity of the nucleotide. One would expect, therefore, that the system relaxes from this perturbation by a diffusion of external water molecules from the bulk solvent into the nucleotide-binding site. Such a diffusion of water molecules has indeed been observed in our simulations. Fig. 5 represents the trajectories of water molecules that make contact with the phosphate tails of the nucleotide during simulation. Water molecules were found to enter the phosphate vicinity of the nucleotide along two pathways: 1) intruding at the "front" (as shown in Fig. 1), where the nucleotide base is exposed to the water; 2) intruding at the "back," connecting the β-phosphate of ADP to the solvent.

Water 696 of CTM entered from the front between residues Lys^{18} and Lys^{336}, coordinated with oxygen O_2A of ATP at 10–490 ps and coordinated with Mg^{2+} at 490–500 ps. Waters 937, 702, and 941 (CTM) entered at the same location and coordinated with oxygen O_2A of ATP at 490–500 ps, 30–35 ps, 80–205 ps, and 460–500 ps. Water 580 of CTm entered from the front between residues Val^{30} and Lys^{336} and coordinated with oxygen O_2A of ATP during the period 195–200 ps.

Incidentally, water diffusion at the opposite side of the protein only occurred in the case of the trajectories CDM, CTM, and CDm. Water 406 of CDM entered between

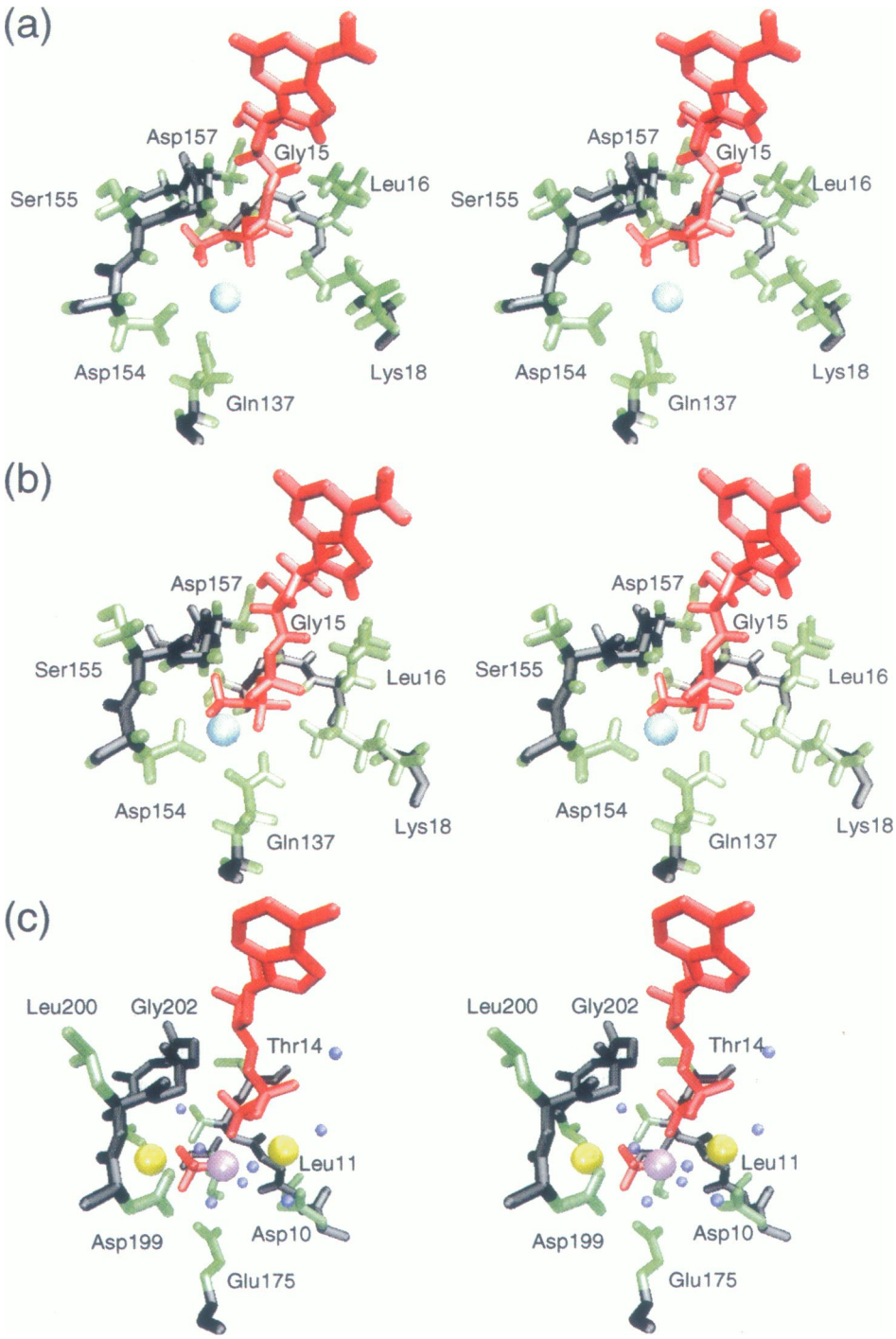

FIGURE 4 Comparison of nucleotide binding sites, visualized by VMD (Humphrey et al., 1996). The nucleotides are shown in red. Ions are represented as spheres: Ca^{2+} in cyan, Mg^{2+} in purple, and K^{+} in yellow. Water oxygens are shown as small blue spheres. The protein backbone is presented in black, and side chains are green. (*a*) ATP binding site of the Kabsch crystal structure (Kabsch et al., 1990). (*b*) ATP binding site of the final structures of CTC. (*c*) ADP-P_i binding site of the chaperone Hsc70 (Wilbanks and McKay, 1995).

residues Val^{159} and Gly^{74} and coordinated with oxygen O1B of ADP at 230–500 ps. Water 731 (CDM) entered from the back between residues Val^{159} and His^{73} and coordinated with oxygen O_3B of ADP at 250–500 ps. Finally, water 465 (CDN) entered from the back between residues Val^{159} and Gly^{74} and coordinated with oxygen O_1B of ADP at 195–300 ps.

Only rarely did one of the 1189 external water molecules enter the phosphate-binding site. Averaged over all seven trajectories, water molecules entered the phosphate vicinity at a rate of 1.5 water molecules per 500 ps simulation time. Fig. 4 shows that in Hsc70 about nine water molecules coordinate the phosphates. The simulation time was too short, therefore, to achieve a significant hydration of the nucleotide-binding site in actin. In addition to the water molecules mentioned, numerous other water molecules diffused into and out of the two channels without coordinating the phosphates or the ion. Such waters have been omitted

TABLE 2 Coordination of the divalent cation: distances in Å between ion and coordinated atoms for ATP structures and ADP structures

ATP-Actin				ADP-Actin			
Atom pair	KAT	CTC	CTM	Atom pair	KAD	CDC	CDM
Ion-OD2 (Asp^{154})	4.73	2.37	1.94	Ion-OD2(Asp^{154})	4.02	2.38	1.90
Ion-OE1 (Gln^{137})	2.96	2.49	2.14	Ion-OE1(Gln^{137})	3.95	2.43	2.02
Ion-O_1A (ATP)	4.56	2.38	1.91	Ion-O_1A(ADP)	4.04	2.37	1.90
Ion-O_1B (ATP)	2.62	2.36	1.91	Ion-O_3B(ADP)	2.46	2.51	1.98
Ion-O_2G (ATP)	2.50	2.23	1.83				

Atom names correspond to PDB nomenclature.

from Fig. 5 for clarity. Based on the observed diffusion of individual water molecules, we suggest the existence of two diffusion pathways on opposite sides of actin's nucleotide-binding site, which provide a solvent connection of the enzymatic pocket to the exterior.

We expect that on time scales much longer than the 500-ps simulation time, the two diffusion pathways would mediate the full hydration of the phosphates and the ion. Furthermore, the pathways could facilitate the exchange of the metal ion and of nucleotide hydrolysis products. The "front door" diffusion pathway may facilitate (accompanied by an opening of the nucleotide-binding cleft; Chik et al., 1996) the docking of the nucleotide, with its highly polar phosphate tail, through the front of the protein; the "back door" diffusion pathway may facilitate the release of the divalent cation and the inorganic phosphate.

Similarity to F-actin

Closure of nucleotide cleft

Given the presumed role of the nucleotide cleft in actin's activity (Lorenz et al., 1993; Tirion et al., 1995; Chik et al., 1996), we followed the separation of the cleft by measuring the distance between the centroids of residues 203–216 (in actin's subdomain 4) and of residues 57–64, 64–69, and 30–33 (in subdomain 2). Fig. 6 shows the cleft separation for the trajectories CDC, CDM, CDN, CTC, and CTM. The nucleotide cleft closed in all trajectories relative to the initial structure. This closure was accompanied by an increase in the number of cross-cleft hydrogen bonds from 18 initially to ~40. The closure is more pronounced in the case of bound Mg^{2+} (closure of 4 Å) compared to bound Ca^{2+} (closure of 2 Å).

Experimental results suggest a magnesium-induced closure of the nucleotide-binding cleft (Strzelecka-Golaszewska et al., 1996). It is believed that Mg^{2+} activates G-actin for polymerization by replacing Ca^{2+} at the high-affinity binding site (Frieden et al., 1980; Carlier, 1991). In the Lorenz F-actin model, the cleft is closed. The closure of the cleft in the F-actin model is similar to the closure observed in our Mg-actin trajectories, measuring 5.8 Å relative to the Kabsch crystal structure. Could the difference between our simulated Ca- and Mg-bound structures imply a Mg-induced conformational activation of actin by cleft closure? Not all of our results support this view. We have started two trajectories (CDm and CTm; see Computational Methods) from Ca-actin trajectories, replacing the divalent cation by Mg^{2+}. The conformations remained very close (cleft closure 2 Å) to those of the corresponding Ca-actin trajectories and did not converge toward the Mg-actin trajectories within 200 ps of simulation. Thus, in our simulation, the actin structure did not differentiate between the cations after closure of the cleft.

Domain movements

To investigate the structural origins of the observed cleft closure, we compared the final structure of CTM as well as the Lorenz F-actin model with the Kabsch crystal structure. For this purpose, we employed the algorithm Hingefind as described in Computational Methods. The results are shown in Fig. 7. The rigid domains identified in the comparison of the final structure of CTM are similar to the rigid domains identified for the F-actin model. In both cases, the largest rigid domain (domain 1) comprises the core of actin's structural subdomains 1 and 3. The two next smallest rigid domains are localized in actin's subdomains 2 and 4. In both systems, we observe a relaxation of subdomain 4 toward the nucleotide-binding cleft and a reorientation of the DNase-binding subdomain 2. Because of the different origin of the exhibited movements, the orientations of the effective hinge axes of subdomain 2 are somewhat different in both cases. In the final structure of CTM, the reorientation of subdomain 2 (a rotation of 10°) is due to the missing DNase-binding contacts. In the case of the Lorenz model, the rotation of 23° is probably caused by interactin docking forces in the filament. Remarkably, the rotation of subdomain 4 (10°), which closes the cleft in F-actin, could be reproduced in our simulation of G-actin (12° rotation in structure from CTM).

Recently, a new crystal structure of actin in an "open" form has been reported (Chik et al., 1996). In this structure subdomain 4 rotates away from the cleft relative to the earlier "classical" crystal structures (Kabsch et al., 1990; Schutt et al., 1993; McLaughlin et al., 1993), opposite to the movement shown in Fig. 7. The conformation reported by Chik et al. confirms that actin's subdomains 1 and 3 (with the exception of a region around Cys374) are relatively

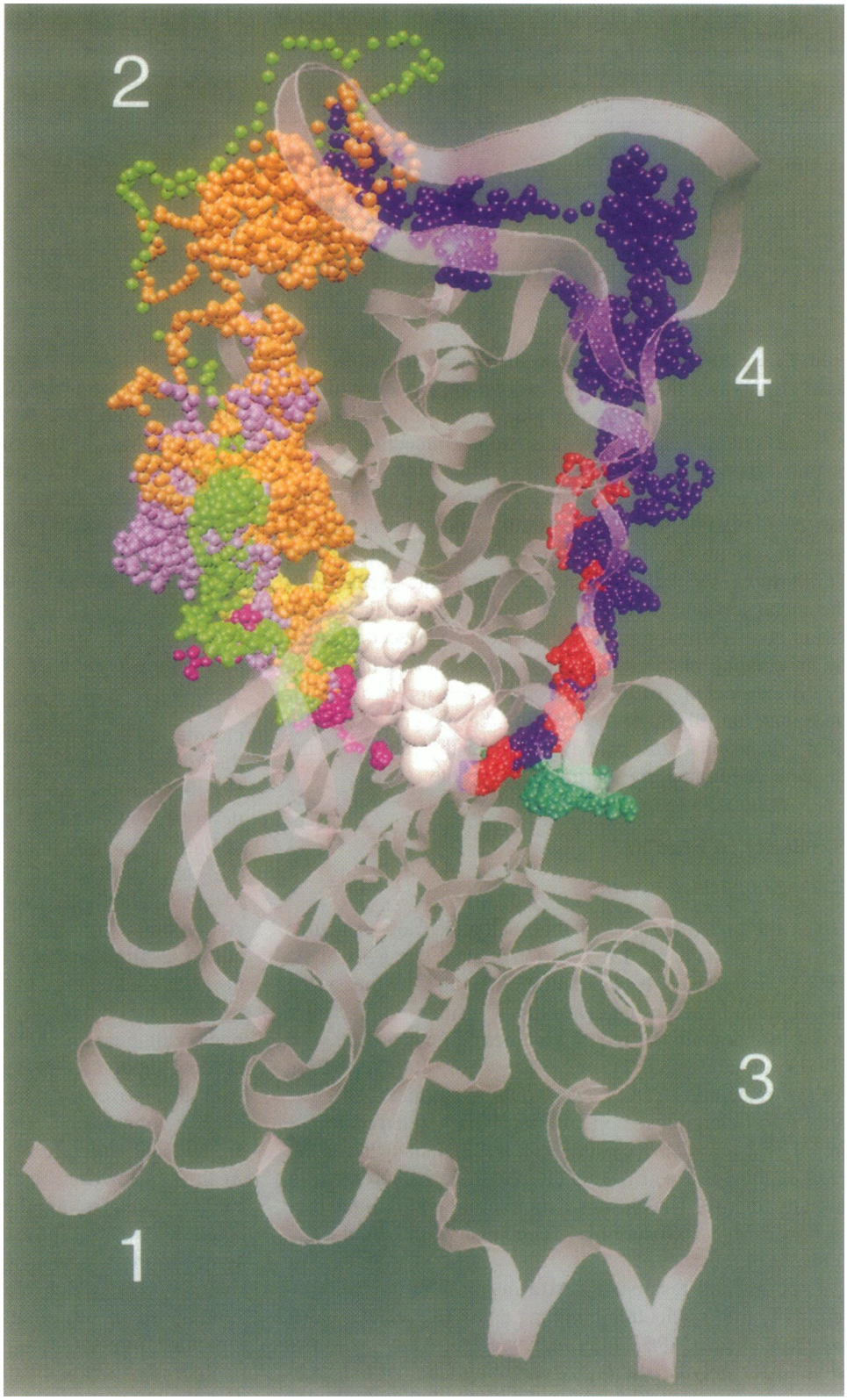

FIGURE 5 Trace of water molecules of various trajectories entering the phosphate vicinity of actin, visualized by VMD (Humphrey et al., 1996). The indices 1–4 identify actin's structural subdomains. Relative to the actin monomer in Fig. 1, the protein is rotated to the left by a 160° rotation about the helical axis. Water oxygen positions are shown as small spheres every 0.1 ps. Positions have been determined by alignment of the trajectories to the Kabsch crystal structure (KAD). *Blue,* water 731 (CDM); *red,* water 406 (CDM); *turquoise,* water 465 (CDN); *purple,* water 696 (CTM); *yellow,* water 702 (CTM); *orange,* water 937 (CTM); *mauve,* water 580 (CTM); *green,* water 941 (CTM). The protein backbone is shown in transparent ribbon representation; ADP and the divalent cation are represented by white van der Waals spheres.

rigid, and that subdomains 2 and 4 swivel by hinged rotations. The domain movements exhibited by actin (Chik et al., 1996; this work) are large compared with those predicted by normal-mode analysis (Tirion and ben-Avraham, 1993). Normal-mode analysis, which predicts soft elastic modes of a protein by harmonic approximation of the atomic interactions (Case, 1994), apparently overestimates the stiffness of the two hinges, as no allowance is made for

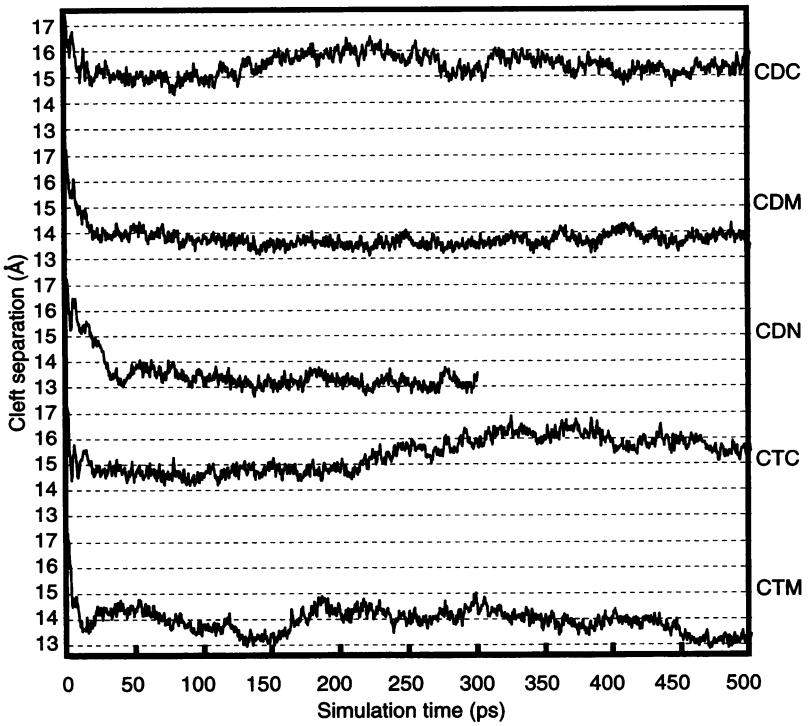

FIGURE 6 Nucleotide cleft separation as a function of simulation time. The initial value was 17.4 Å (for CDC, CDM, CDN, CTC, and CTM). After 50-ps simulation, the cleft separation assumed new average values: 15.4 (± 0.4) Å (CDC), 13.7 (± 0.2) Å (CDM), 13.2 (± 0.3) Å (CDN), 15.4 (± 0.6) Å (CTC), and 13.9 (± 0.4) Å (CDC).

the (unharmonic) relaxation of conformational strains (Karplus and McCammon, 1983). The difference in energy between the open form and the classical form of actin is only a fraction of thermal energy (Chik et al., 1996). This slight difference reveals an extreme sensitivity of actin's conformation to changes in the environment. The open- and closed-cleft conformations of actin (Chik et al., 1996; this work) can thus be interpreted as instances in an ensemble of thermally accessible conformations.

Classification of structures

In Fig. 8 we have classified the conformations of all available actin structures according to the radius of gyration and cleft separation to investigate their conformational resemblance with F-actin. Conformations from MD simulation were selected from the trajectories at 300 and 500 ps. The radius of gyration (Eq. 2) provides a measure of the compactness of a protein. This measure is particularly useful here because it distinguishes the structure according to the radial location of flexible loops, such as the DNase-binding loop 38–52 and the "hydrophobic plug" loop 264–273, which are relevant for the function of the protein.

We interpret the distribution of structures as follows. The structures with bound Ca^{2+} (CDC and CTC) fall into a cluster of states near the Schutt crystal structure (SCH). The structures with bound Mg^{2+} (CDM, CDN, and CTM) exhibit a smaller cleft separation and branch into two clusters. Most structures are found along a diagonal line that links the crystal structures (KAD/KAT and SCH) to structures with small cleft separation. A narrower cleft and the relaxation of the DNase-binding loop 38–52 yield a more compact and globular protein. Thus the radius of gyration and the cleft separation of many states are correlated along the diagonal line in Fig. 8. In addition to these crystal-like states, a second cluster of states comprising the CDN and CTM structures is located at a radius of gyration of 22 Å. These structures, which bridge the gap from the crystal conformations to the Lorenz F-actin model, will be referred to as *G-F intermediates*. No simulated structure was found near the Tirion F-actin model, which exhibits a rather large radius of gyration due to a different orientation of subdomain 2 (Tirion et al., 1995).

Hydrophobic plug release

To find a structural basis for the observed conformational changes of actin, we determined first-order contributions of individual residues to differences in radii of gyration, Δr_{gyr}, employing Eq. 4. In Fig. 9, first-order contributions of selected simulated structures and of the Lorenz F-actin model are compared with the Kabsch crystal structure. We found that higher order contributions in the expansion in Eq. 5 typically result in an error of less than 0.05 Å for the difference in r_{gyr}. This absolute error is roughly on the order of single residue contributions, a small value considering the large fluctuation of the Δr_{gyr} values in Fig. 9.

Residues of actin's subdomain 2 (residues 33–69), notably the DNase binding loop 38–52, generally are at a smaller radius compared to the Kabsch crystal structure, because of a relaxation of the loop from missing crystal contacts with DNase. Residues 200–250 of actin's subdomain 4 exhibit noticeable fluctuations in the Δr_{gyr} contributions due to the closure of the cleft in the simulated

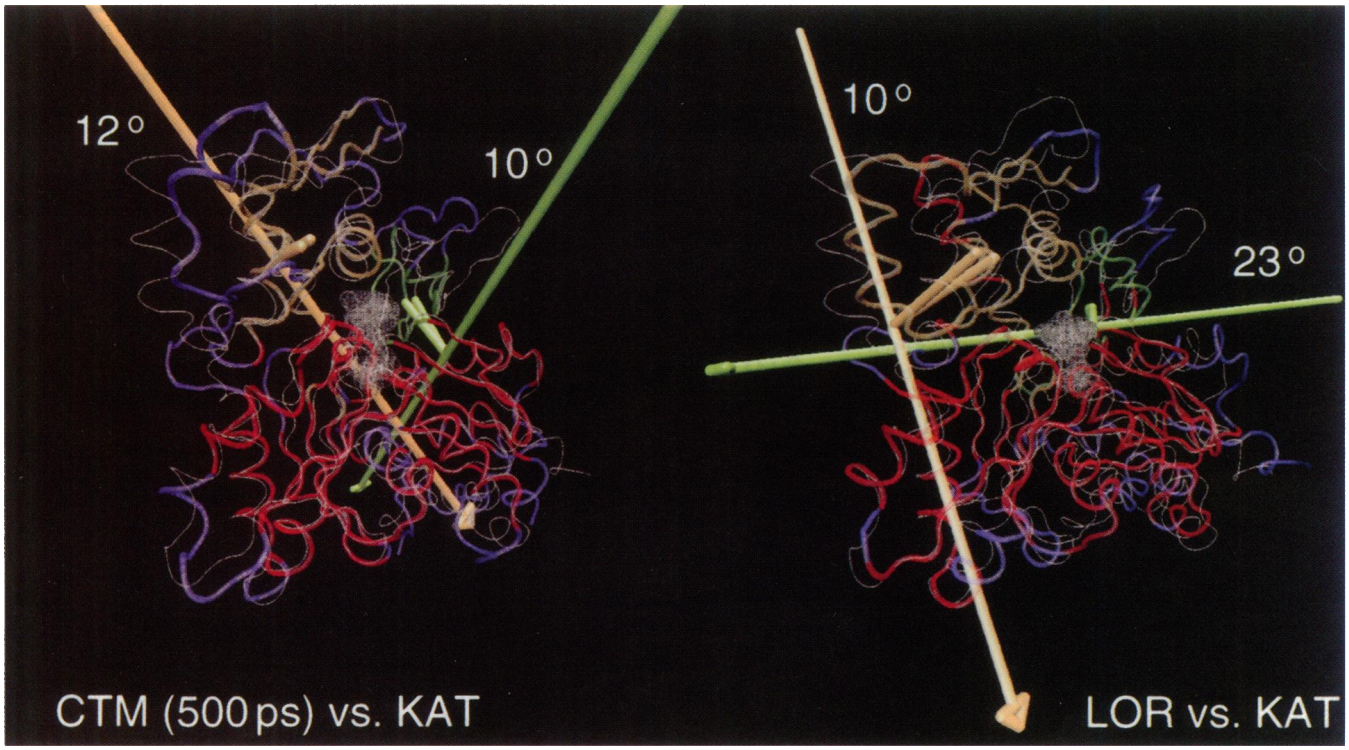

FIGURE 7 Actin domain movements as determined by Hingefind (Wriggers and Schulten, 1997), visualized by VMD (Humphrey et al., 1996). Colored backbone traces of the final structure of CTM (*left*) and of the Lorenz F-actin model (LOR, *right*) are superimposed on the trace of the Kabsch crystal structure (KAT, *white line*) by matching the largest rigid domain found (*red*). The resolution of the Hingefind domain partitioning, 1.8 Å (*left*) and 3.0 Å (*right*), was chosen to obtain the same level of detail for both comparisons. The reference domain (*red*) comprises mainly residues of actin's subdomains 1 and 3. The movements of the two next largest domains (*orange, green*) relative to the reference domain have been visualized by the effective rotation axes (hinges), which indicate a left-handed rotation relative to the crystal structure. The angles of the respective rotations are given. The ATP nucleotide and Mg^{2+} ion are presented as white transparent van der Waals spheres. Blue tubes indicate regions that are disordered.

structures, which is accompanied by a rotation of subdomain 4 (Fig. 7). As can be expected, lateral movements, as exhibited by subdomain 4, are not well characterized by the Δr_{gyr} contributions. Loop 264–273 is at a larger radius compared to the crystal structure in the simulated structures from the *G-F intermediate* trajectories CTM and CDN. Obviously, this displacement is most pronounced in the LOR structure, where the loop was remodeled to form a protruding β-hairpin. On the other hand, the structures from the trajectories CDC, CTC, and CTM do not indicate any

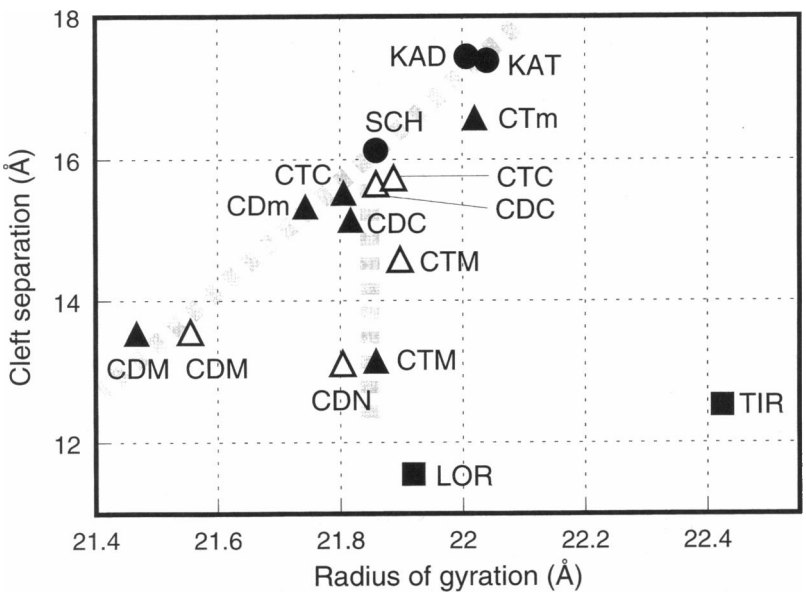

FIGURE 8 Comparison of conformational properties of investigated structures according to radius of gyration and cleft separation. ●, G-actin crystal structures; ■, F-actin model structures; △, structures after 300-ps simulation; ▲, structures after 500-ps simulation. The radii of gyration of KAD, KAT, and TIR, which each have three residues missing, were extrapolated to 375 residues by a scaling factor of 1.0015, estimated from simulated structures. Two clusters of conformational states can be identified and are represented by dashed bars in the diagram.

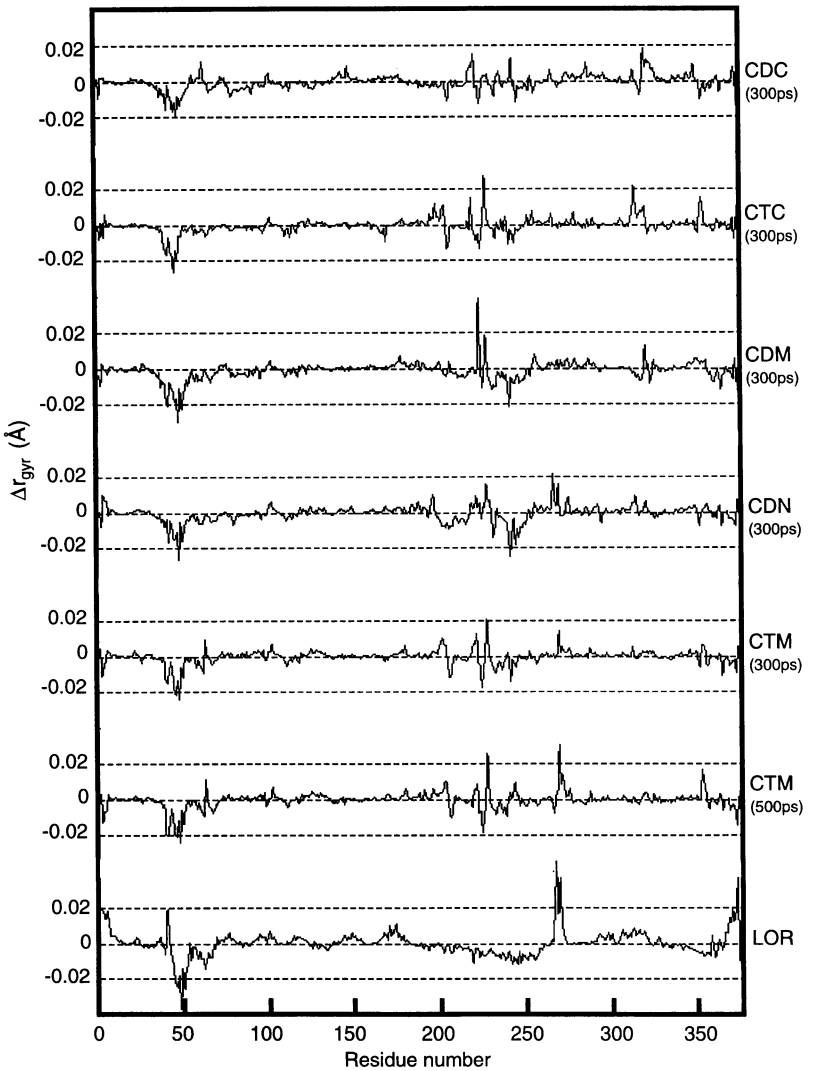

FIGURE 9 First-order contributions to differences in radius of gyration, Δr_{gyr}, of residues from simulated structures and from the Lorenz F-actin model relative to the Kabsch crystal structure (KAD). The contributions from Eq. 4 have been summed up for each residue. For simulated structures, the simulation time is indicated.

radial differences in loop 264–273 relative to the crystal structure. Differences in the two conformational clusters of Fig. 8 thus appear to originate from a detachment of the loop 264–273 from the main body of the protein in the G-F intermediate states.

Fig. 10 illustrates the conformation of loop 264–273 in the Kabsch crystal structure, in the Lorenz F-actin model, and in the trajectories CTM and CDC after 500-ps simulation. In CDC, the loop remains packed against the main body of the protein, similar to the Kabsch crystal structure. The final structure of CTM represents the detached state of the loop in the G-F intermediate states. An inspection of the binding contacts of the loop at the interface of subdomains 3 and 4 revealed that the position of the carboxylate side chain of Glu^{259} in the initial crystal structure (Kabsch et al., 1990) facilitates the detachment, as it prevents Phe^{266} from forming stable hydrophobic interactions with Met^{227} and Phe^{223}. The rotation of subdomain 4 associated with cleft closure further destabilized the binding contacts of the loop at the interface of subdomains 3 and 4 (Fig. 7). Because the loop became detached in the G-F intermediate conformations only, it appears that there is a correlation between detachment of the loop and the closure of the cleft by rotation of subdomain 4. A restructuring of the loop into a β-hairpin, as in the Lorenz model of F-actin (Holmes et al., 1990), was not observed. The docking of the loop into the hydrophobic cavity of the opposing F-actin strand may be required for the β-hairpin conformation to be energetically favorable.

SUMMARY AND CONCLUSIONS

In the following we will interpret our findings in terms of actin's function in cell motility. First, we will discuss implications of the observed water diffusion pathways for the exchange of substrates in the ATP hydrolysis reaction and, in particular, for the release of inorganic phosphate. We will then consider questions of ion binding to actin's enzymatic site, namely, if monovalent ions bind to the site similar to the protein Hsc70, and how the divalent cation controls cleft closure. We will show that the observed detachment of the

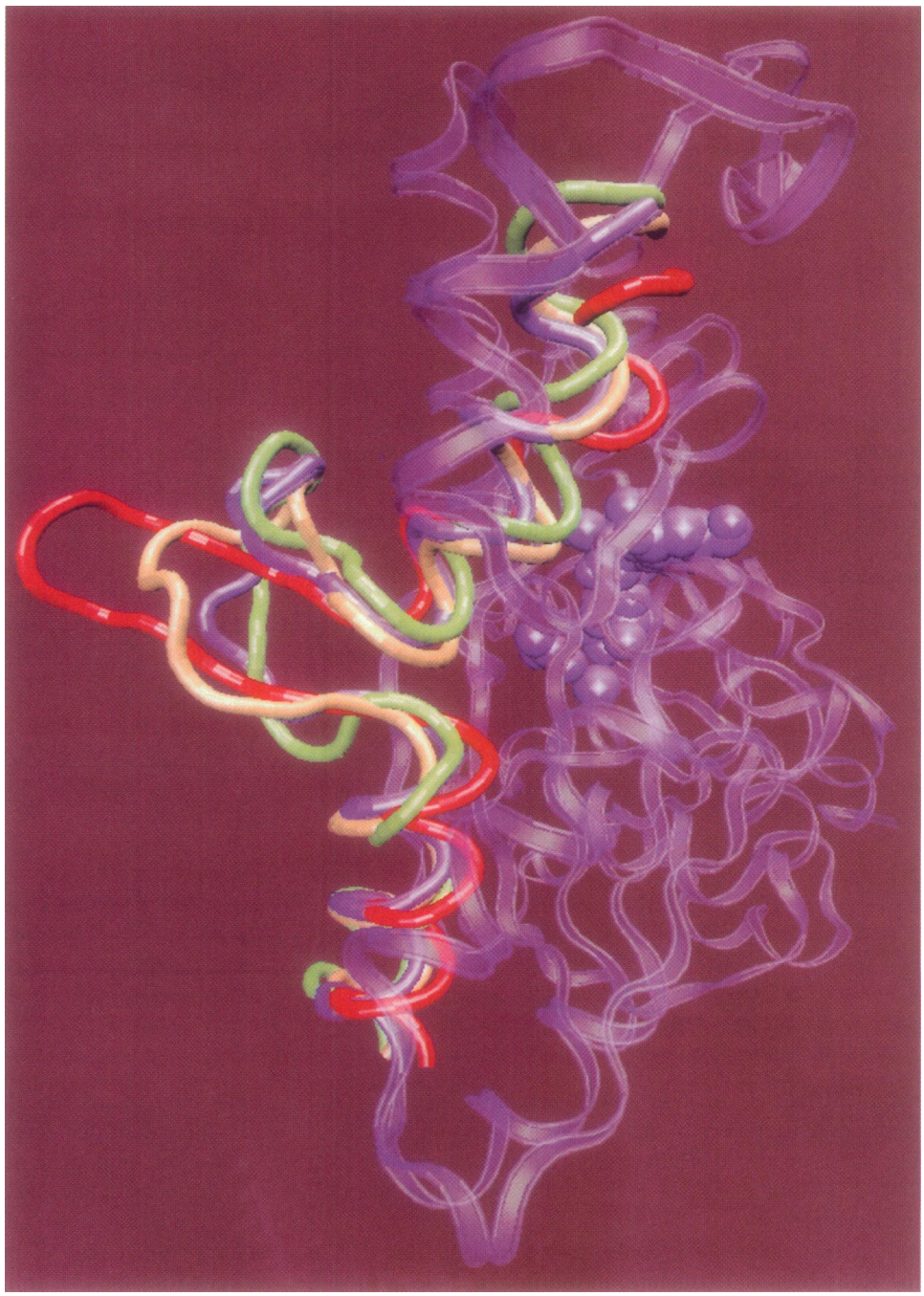

FIGURE 10 Conformation of the "hydrophobic plug" loop 264–273 in four structures aligned with the Kabsch crystal structure (KAT), visualized by VMD (Humphrey et al., 1996). The backbone of residues 253–285 is shown as a colored tube in each case. *Green,* final structure of CDC; *blue,* KAT; *red,* LOR; *brown,* final structure of CTM. The protein backbone is shown in transparent ribbon representation; ATP and divalent cations are represented by van der Waals spheres.

subdomain 3/4 loop 264–273 and structural similarities to F-actin may explain aspects of actin's G-F conformational transition and the effect of polymerization on ATPase activity.

The observed diffusion of water molecules into the nucleotide-binding site suggests a new model for actin's ATPase activity. The nucleotide is exchanged through the front of the protein, where the base is exposed to the exterior; the inorganic phosphate is released through the back-door diffusion pathway after ATP hydrolysis. A back-door mechanism of enzyme function was first suggested by Mitchell and Moyle (1958). The authors argued that ATPases can serve as reactants in group-transfer reactions. An anisotropy of the catalytic regions of the enzyme molecule and a transport of the phosphate to the opposite side of the nucleotide phase were predicted. More recently, back-door mechanisms have been suggested for tryptophan synthase (Hyde et al., 1988), acetylcholinesterase (Gilson et al., 1994), and the motor protein myosin (Yount et al., 1995). Other likely candidates are the α-subunit of G-proteins (Coleman et al., 1994) and the Ras-related protein Rap1A (Nassar et al., 1995). Two experimental results suggest that the proposed "back-door" diffusion pathway may assist actin's enzymatic activity: 1) at low metal ion concentra-

tions, the tightly bound divalent cation is able to dissociate from the protein (Kinosian et al., 1993), apparently through an unbinding channel different from the one used for nucleotide exchange, leaving behind a stable divalent-cation-free nucleotide (Valentin-Ranc and Carlier, 1991); 2) in the Lorenz F-actin model (Lorenz et al., 1993), the poison phalloidin is predicted to bind near the exit (residue His^{73}) of the putative "back-door" pathway, where it would interfere with the water diffusion (cf. Figs. 1 and 5). If the inorganic phosphate leaves actin along the "back door" pathway, one would expect a phalloidin-induced delay of phosphate release, which, indeed, has been observed experimentally (Dancker and Hess, 1990).

In addition to water molecules, the structure of the ATPase domain of Hsc70, which is homologous to actin, contains two monovalent ions in the enzymatic pocket (Fig. 4). One question we did not address in the present study is whether ions play a role in actin's activity as well. Little is known about the effects of monovalent cations on actin activity. It is conceivable that in the case of actin such monovalent ions could have remained undetected in the reported (>2.5-Å resolution) structures (Kabsch et al., 1990; Schutt et al., 1993; McLaughlin et al., 1993; Chik et al., 1996), as this was the case in earlier crystal structures of Hsc70 (Flaherty et al., 1990, 1994). It is firmly established (Kinosian et al., 1993) that nucleotide exchange from actin monomers is more rapid at low (1–10 μM) than at high (>100 μM) divalent cation concentrations when the potassium concentration is low and constant. Raising the potassium and magnesium concentrations simultaneously abolishes the inhibition by the divalent cation (Pollard et al., 1992). De la Cruz and Pollard have found that the dissociation rate constant of ATP from Mg-ATP-actin monomers increases from 0.0045 s^{-1} at 0 KCl to 0.020 s^{-1} at 200 mM KCl (de la Cruz and Pollard, personal communication). (Conditions: 1 mM $MgCl_2$, 20 mM Tris (pH 8.0), temperature 22°C, 0 free ATP, 200 μM ethenoATP.) One interpretation of these results is that potassium ions compete with magnesium for binding to the high-affinity nucleotide and divalent cation-binding site, lowering the effective Mg^{2+} concentration and increasing the rate of nucleotide exchange. Potassium ion-binding sites in the central enzymatic pocket of actin would be consistent with the kinetic data.

The more pronounced cleft closure of simulated Mg-actin relative to Ca-actin is the result of differences in the energetic parameters of a sole atom. The central location of the enzymatic pocket enables actin to mediate and amplify small structural differences throughout the protein. The effect of missing solvent molecules in the crystal structure on the cleft closure is, however, not known. Therefore our present results remain inconclusive regarding the detailed structure of Mg-actin.

Surprisingly, the conformations of Mg-actin in our simulations resemble the putative F-actin structure in terms of cleft closure and domain movement. Our results suggest that the structural changes attributed to the G-F transition (Lorenz et al., 1993; Tirion et al., 1995), notably the closure of the cleft by a rotation of subdomain 4, destabilize the binding contacts of loop 264–273. This may be interpreted as a preparative step in the more extensive structural transition of the loop, forming a plug upon binding to the hydrophobic cavity in the opposing strand of the actin filament (Holmes et al., 1990). The simulations also indicate that the interaction of Glu^{259} with Phe^{266} in the Kabsch crystal structure facilitates the detachment of the loop. In the actin:profilin and actin:gelsolin-subfragment 1 structures (Schutt et al., 1993; McLaughlin et al., 1993; Chik et al., 1996), Glu^{259} formed a salt bridge with Arg^{312}. Our results provide a plausible scenario for the loop detachment, assuming that salt bridge 259–312 breaks in the polymerization of actin, so that the arrangement of residues used in this work has functional significance. Schutt and co-workers question whether this salt bridge can break (Schutt et al., 1993, 1994; Chik et al., 1996), suggesting that the loop does not detach from the protein. Unpublished simulations with the actin:gelsolin-subfragment 1 structure (McLaughlin et al., 1993) indicate that the salt bridge is stable on the picosecond to nanosecond time scale. This comes as no surprise, given the limited simulation time. Hence our results are inconclusive regarding Schutt's suggestion. Mutational experiments, however, indicating a cold-sensitive polymerization defect of the L266D mutant (Chen et al., 1993; Kuang and Rubenstein, 1997a; Kuang and Rubenstein, 1997b), are in favor of the plug hypothesis.

Crystal structures of proteins frequently do not exhibit water molecules, because of an insufficient resolution of the diffraction data or the high mobility of the water molecules. Does the unexpected similarity of our simulated structures to the Lorenz F-actin model in terms of cleft closure and domain movement originate from the observed dehydration and compaction of the nucleotide-binding site? Although we cannot rule out that other effects, such as the instability of the "hydrophobic plug" loop or missing monovalent ions in the structure, contribute to the observed movements, a causal connection between nucleotide hydration and cleft separation is likely for two reasons. First, the nucleotide-binding site in the open-cleft structure of actin (Chik et al., 1996) was shown to be more solvent accessible. Second, a dehydration of the nucleotide-binding site in F-actin would be consistent with one important aspect of actin's enzymatic activity: the ATPase activity increases when actin monomers polymerize into filaments (Allen et al., 1996). Because of large distances between the nucleotide and residues in the enzymatic pocket (Table 2), actin's crystal structure does not reveal the catalytic mechanism (Holmes and Kabsch, 1991). A compaction of the enzymatic site, induced by a closure of the cleft during polymerization, could drive out water molecules and put catalytic residues in a place that promotes the hydrolysis of the phosphate.

The placement of missing buried waters in the actin crystal structure will provide a basis for future simulations. The actin filament structure, however, constitutes the most challenging problem in the modeling of the protein. Al-

though computer simulations of biomelocular systems of 100,000 atoms now become feasible, induced-fit conformational changes in the docking of actin monomers during polymerization, and effects of the nucleotide on actin's propensity to aggregate, can only be simulated directly once an accurate model of the filament becomes available. The refinement of actin against x-ray fiber diffraction data at 8-Å resolution (Lorenz et al., 1993) still leaves much room for maneuver for local main-chain and side-chain conformations that determine the binding interfaces (Fig. 1). It is our hope that in the near future, new experimental results will yield an optimization of interactin contacts in Cartesian space, which could be combined with an optimization of the filament structure in the reciprocal space of x-ray fiber diffraction (Lorenz et al., 1993). Such data would permit the investigation of the dynamics of F-actin at atomic resolution.

We thank Enrique de la Cruz and Thomas D. Pollard for measuring the effect of potassium on nucleotide dissociation and sharing their results before publication. We thank Wolfgang Kabsch, Michael D. Rozycki, Michael Lorenz, and Monique M. Tirion for providing the actin structures used in this work, and Marie-France Carlier, Robert M. Jones, and Alex D. MacKerell for useful suggestions and comments.

This work was supported by National Institutes of Health grant PHS 5 P41 RR05969-04, National Science Foundation grants BIR 9318159 and BIR 9423827 (EQ), the Roy J. Carver Charitable Trust, and a MCA 93S028P computer time grant at the Pittsburgh Supercomputing Center.

REFERENCES

Allen, P. G., L. E. Laham, M. Way, and P. A. Janmey. 1996. Binding of phosphate, aluminum fluoride, or beryllium fluoride to F-actin inhibits severing by gelsolin. *J. Biol. Chem.* 271:4665–4670.

Breed, J., R. Sankararamakrishnan, I. D. Kerr, and M. S. P. Sansom. 1996. Molecular dynamics simulations of water within models of ion channels. *Biophys. J.* 70:1643–1661.

Brooks, B. R., R. E. Bruccoleri, B. D. Olafson, D. J. States, S. Swaminathan, and M. Karplus. 1983. CHARMm: a program for macromolecular energy, minimization, and dynamics calculations. *J. Comp. Chem.* 4:187–217.

Brünger, A. T. 1992. X-PLOR, Version 3.1: A System for X-ray Crystallography and NMR. The Howard Hughes Medical Institute and Department of Molecular Biophysics and Biochemistry, Yale University, New Haven, CT.

Carlier, M.-F. 1991. Actin: protein structure and filament dynamics. *J. Biol. Chem.* 266:1–4.

Case, D. A. 1994. Normal mode analysis of protein dynamics. *Curr. Opin. Struct. Biol.* 4:285–290.

Chen, X., R. K. Cook, and P. A. Rubenstein. 1993. Yeast actin with a mutation in the "hydrophobic plug" between subdomains 3 and 4 ($L_{266}D$) displays a cold-sensitive polymerization defect. *J. Cell Biol.* 123:1185–1195.

Chik, J. K., U. Lindberg, and C. E. Schutt. 1996. The structure of an open state of beta actin at 2.65 Å resolution. *J. Mol. Biol.* 263:607–623.

Coleman, D. E., A. M. Berghuis, E. Lee, M. E. Linder, A. G. Gilman, and S. R. Sprang. 1994. Structures of active conformations of $G_{i\alpha 1}$ and the mechanism of GTP hydrolysis. *Science.* 265:1405–1412.

Coluccio, L. M., and L. G. Tilney. 1984. Phalloidin enhances actin assembly by preventing monomer dissociation. *J. Cell Biol.* 99:529–535.

Daggett, V., and M. Levitt. 1993. Realistic simulations of native-protein dynamics in solution and beyond. *Annu. Rev. Biophys. Biomol. Struct.* 22:353–380.

Dancker, P., and L. Hess. 1990. Phalloidin reduces the release of inorganic phosphate during actin polymerization. *Biochim. Biophys. Acta.* 1035: 197–200.

de la Cruz, E. M., and T. D. Pollard. 1994. Transient kinetic analysis of rhodamine phalloidin binding to actin filaments. *Biochemistry.* 33: 14387–14392.

Devreotes, P. N., and S. H. Zigmond. 1988. Chemotaxis in eukaryotic cells: a focus on leukocytes and *Dictyostelium*. *Annu. Rev. Cell Biol.* 4:649–686.

Estes, J. E., L. A. Selden, and L. C. Gershman. 1981. Mechanism of action of phalloidin on the polymerization of muscle actin. *Biochemistry.* 20:708–712.

Flaherty, K. M., C. DeLuca-Flaherty, and D. B. McKay. 1990. Three-dimensional structure of the ATPase fragment of a 70K heat-shock cognate protein. *Nature.* 346:623–628.

Flaherty, K. M., D. McKay, W. Kabsch, and K. C. Holmes. 1991. Similarity of the three-dimensional structures of actin and the ATPase fragment of a 70-kDa heat shock cognate protein. *Proc. Natl. Acad. Sci. USA.* 88:5041–5045.

Flaherty, K. M., S. M. Wilbanks, C. DeLuca-Flaherty, and D. B. McKay. 1994. Structural basis of the 70-kilodalton heat shock cognate protein ATP hydrolytic activity. *J. Biol. Chem.* 269:12899–12907.

Frieden, C., D. Lieberman, and H. R. Gilbert. 1980. A flourescent probe for conformational changes in skeletal muscle G-actin. *J. Biol. Chem.* 255: 8991–8993.

Frisch, M. J., G. W. Trucks, M. Head-Gordon, P. M. W. Gill, M. W. Wong, J. B. Foresman, B. G. Johnson, H. B. Schlegel, M. A. Robb, E. S. Replogle, R. Gomperts, J. L. Andres, K. Raghavachari, J. S. Binkley, C. Gonzalez, R. L. Martin, D. J. Fox, D. J. Defrees, J. Baker, J. J. P. Stewart, and J. A. Pople. 1992. Gaussian 92, Revision A. Gaussian, Inc., Pittsburgh, PA.

Gilson, M. K., T. P. Straatsma, J. A. McCammon, D. R. Ripoll, C. H. Faerman, P. H. Axelsen, I. Silman, and J. L. Sussman. 1994. Open "back door" in a molecular dynamics simulation of acetylcholinesterase. *Science.* 263:1276–1278.

Guàrdia, E., and J. A. Padró. 1996. On the structure and dynamic properties of aqueous solutions: molecular dynamics simulation of Cl^- and Cl^{2-} in water. *Mol. Simulation.* 17:83–94.

Holmes, K. C., and W. Kabsch. 1991. Muscle proteins: actin. *Curr. Opin. Struct. Biol.* 1:270–280.

Holmes, K. C., D. Popp, W. Gebhard, and W. Kabsch. 1990. Atomic model of the actin filament. *Nature.* 347:44–49.

Humphrey, W. F., A. Dalke, and K. Schulten. 1996. VMD—visual molecular dynamics. *J. Mol. Graphics.* 14:33–38.

Hyde, C. C., S. A. Ahmed, E. A. Padlan, E. W. Miles, and D. R. Davies. 1988. Three-dimensional structure of the tryptophan synthase $\alpha_2\beta_2$ multienzyme complex from *Salmonella typhimurium*. *J. Biol. Chem.* 263:17857–17871.

Isambert, H., P. Venier, A. C. Maggs, A. Fattoum, R. Kassab, D. Pantaloni, and M. F. Carlier. 1995. Flexibility of actin filaments derived from thermal fluctuations. *J. Biol. Chem.* 270:11437–11444.

Israelachvili, J. N. 1992. Intermolecular and Surface Forces. Academic Press, London.

Jorgensen, W. L., J. Chandrasekhar, J. D. Madura, R. W. Impey, and M. L. Klein. 1983. Comparison of simple potential functions for simulating liquid water. *J. Chem. Phys.* 79:926–935.

Kabsch, W. 1976. A solution for the best rotation to relate two sets of vectors. *Acta Crystallogr. A.* 32:922–923.

Kabsch, W., H. Mannherz, D. Suck, E. Pai, and K. Holmes. 1990. Atomic structure of the actin: DNase I complex. *Nature.* 347:37–44.

Karplus, M., and J. A. McCammon. 1983. Dynamics of proteins: elements and function. *Annu. Rev. Biochem.* 53:263–300.

Kinosian, H. J., L. A. Selden, J. E. Estes, and L. C. Gershman. 1993. Nucleotide binding to actin. *J. Biol. Chem.* 268:8683–8691.

Kuang, B., and P. A. Rubenstein. 1997a. Beryllium fluoride and phalloidin restore polymerizability of a mutant yeast actin (V266G, L267G) with severely decreased hydrophobicity in a subdomain 3/4 loop. *J. Biol. Chem.* 272:1237–1247.

Kuang, B., and P. A. Rubenstein. 1997b. The effects of severely decreased hydrophobicity in a subdomain 3/4 loop on the dynamics and stability of yeast G-actin. *J. Biol. Chem.* 272:4412–4418.

Levitt, M. 1983. Molecular dynamics of native protein. *J. Mol. Biol.* 168:595–620.

Lorenz, M., D. Popp, and K. C. Holmes. 1993. Refinement of the F-actin model against X-ray fiber diffraction data by the use of a directed mutation algorithm. *J. Mol. Biol.* 234:826–836.

McLaughlin, P. J., J. T. Gooch, H.-G. Mannherz, and A. G. Weeds. 1993. Structure of gelsolin segment 1-actin complex and the mechanism of filament severing. *Nature.* 364:685–692.

Mitchell, P., and J. Moyle. 1958. Enzyme catalysis and group translocation. *Proc. R. Phys. Soc. Edinb.* 27:61–72.

MSI. 1994. QUANTA 4.0. Molecular Simulations, Inc., Burlington, MA.

Nassar, N., G. Horn, C. Herrmann, A. Scherer, F. McCormick, and A. Wittinghofer. 1995. The 2.2 Å crystal structure of the ras-binding domain of the serine/threonine kinase c-Raf1 in complex with Rap1A and a GTP analogue. *Nature.* 375:554–560.

Pollard, T. D., I. Goldberg, and W. H. Schwarz. 1992. Nucleotide exchange, structure, and mechanical properties of filaments assembled from ATP-actin and ADP-actin. *J. Biol. Chem.* 267:20339–20345.

Sampath, P., and T. D. Pollard. 1991. Effects of cytochalasin, phalloidin, and pH on the elongation of actin filaments. *Biochemistry.* 30: 1973–1980.

Schutt, C. E., J. C. Myslik, M. D. Rozycki, N. C. W. Goonesekere, and U. Lindberg. 1993. The structure of crystalline profilin-β-actin. *Nature.* 365:810–816.

Schutt, C. E., M. D. Rozycki, and U. Lindberg. 1994. What's the matter with the ribbon. *Curr. Biol.* 4:185–186.

Small, J. V. 1989. Microfilament-based motility in non-muscle cells. *Curr. Opin. Cell Biol.* 1:75–79.

Steinbach, P. J., and B. R. Brooks. 1993. Protein hydration elucidated by molecular dynamics simulation. *Proc. Natl. Acad. Sci. USA.* 90: 9135–9139.

Strzelecka-Golaszewska, H., A. Wozniak, T. Hult, and U. Lindberg. 1996. Effects of the type of divalent cation, Ca^{2+} or Mg^{2+}, bound at the high-affinity site and of the ionic composition of the solution on the structure of F-actin. *Biochem. J.* 316:713–721.

Suda, H., and M. Saito. 1994. Molecular dynamics simulations for actin monomers in solution. *J. Theor. Biol.* 171:347–349.

Teeter, M. M. 1991. Water-protein interactions: theory and experiment. *Annu. Rev. Biophys. Biophys. Chem.* 20:577–600.

Theriot, J. A., T. J. Mitchison, L. G. Tilney, and D. A. Portnoi. 1992. The rate of actin-based motility of intracellular *Listeria monocytogenes* equals the rate of actin polymerization. *Nature.* 357:257–260.

Tirion, M. M., and D. ben-Avraham. 1993. Normal mode analysis of G-actin. *J. Mol. Biol.* 230:186–195.

Tirion, M. M., D. ben-Avraham, M. Lorenz, and K. C. Holmes. 1995. Normal modes as refinement parameters for the F-actin model. *Biophys. J.* 68:5–12.

Valentin-Ranc, C., and M.-F. Carlier. 1991. Role of ATP-bound divalent metal ion in the conformation and function of actin. *J. Biol. Chem.* 266:7668–7675.

Ward, G. 1994. The Radiance Lighting Simulation and Rendering System. Computer Graphics, Orlando, FL.

Wilbanks, S. M., and D. B. McKay. 1995. How potassium affects the activity of the molecular chaperone Hsc70. *J. Biol. Chem.* 270: 2251–2257.

Wriggers, W., and K. Schulten. 1997. Protein domain movements: detection of rigid domains and visualization of hinges in comparisons of atomic coordinates. *Proteins Struct. Funct. Genet.* (in press).

Yount, R. G., D. Lawson, and I. Rayment. 1995. Is myosin a "back door" enzyme? *Biophys. J.* 68:44s–49s.

Zhang, L., and J. Hermans. 1996. Hydrophilicity of cavities in proteins. *Proteins Struct. Funct. Genet.* 24:433–438.